*macromol*

MDPI

*Article*

# Photocatalytic Performance of Niobium Oxyhydroxide/ Poly(butylene adipate-co-terephthalate) Composites for Dye Methylene Blue Degradation in Aqueous Media

**Maria Eduarda Soares Pinheiro [1], Ana Pacheli Heitmann [1,2], Letícia Costa Martins [1], Jhonatan Bispo de Oliveira [1], Ildefonso Binatti [1], Emerson Fernandes Pedroso [1], Rodinei Augusti [1], Patterson Patricio de Souza [1], Luiz Carlos Alves de Oliveira [2] and Patricia Santiago de Oliveira Patricio [1,*]**

[1] IntechLab Laboratory, Departamento de Química, Universidade Federal de Ciência e Inovação de Minas Gerais, UFCIMG, Av. Amazonas 5253, Belo Horizonte 30421-169, MG, Brazil; madusp@outlook.com (M.E.S.P.); anapacheli@gmail.com (A.P.H.); cmleticia13@gmail.com (L.C.M.); jhonatanbo@hotmail.com (J.B.d.O.); binatti@cefetmg.br (I.B.); pedroso@cefetmg.br (E.F.P.); augusti.rodinei@gmail.com (R.A.); patterson@cefetmg.br (P.P.d.S.)

[2] Departamento de Química, Instituto de Ciências Exatas, Universidade Federal de Minas Gerais, Avenida Antônio Carlos, 6627, Belo Horizonte 31270-901, MG, Brazil; lcao.ufmg@gmail.com

* Correspondence: patricia@cefetmg.br

## Abstract

Immobilizing semiconductor photocatalysts in polymeric matrices has emerged as an effective strategy to overcome one of the main limitations of heterogeneous photocatalysis: recovering and reusing powdered catalysts after wastewater treatment. In this study, biodegradable poly(butylene adipate-co-terephthalate) (PBAT) was used as a support for niobium oxyhydroxide (S2) to produce photocatalytic composites by melt extrusion followed by hot pressing. The materials were characterized by Fourier-transform infrared spectroscopy (FTIR), thermogravimetric analysis (TGA), and differential scanning calorimetry (DSC), and their photocatalytic performance was evaluated by measuring methylene blue degradation under UV irradiation. FTIR analyses indicated interfacial interactions between PBAT and niobium oxyhydroxide without compromising the polymer structure. Thermal analyses showed that incorporating the catalyst preserved the thermal stability and processability of the composites. Among the formulations investigated, the composite containing 95 wt% PBAT, 5 wt% S2, and an additional surface deposition of 0.2 g of catalyst exhibited the highest photocatalytic performance, achieving approximately 88% methylene blue removal within 120 min. The improved efficiency was attributed to the synergistic contribution of adsorption and photocatalytic oxidation, promoted by accessible catalytically active sites and the generation of reactive oxygen species. Electrospray ionization mass spectrometry confirmed the progressive oxidative degradation of methylene blue. In addition to efficiently removing pollutants, immobilizing S2 on a biodegradable polymer matrix enables simple catalyst recovery. This approach offers a sustainable alternative for advanced oxidation processes aimed at wastewater remediation.

**Keywords:** biodegradable composites; poly(butylene adipate-co-terephthalate); niobium oxyhydroxide; photocatalysis; methylene blue

Received: 10 September 2026
Revised: 11 November 2026
Accepted: 18 November 2026
Published: 21 November 2026

**Copyright:** © 2026 by the authors. Licensee MDPI, Basel, Switzerland. This article is an open access article distributed under the terms and conditions of the Creative Commons Attribution (CC BY) license.

## 1. Introduction

In recent years, water resource contamination has emerged as one of the most critical environmental concerns, driven and intensified by both natural sources and anthropogenic activities [1,2]. Synthetic organic dyes are widely used across sectors including the textile, cosmetic, food, and medical industries [3–5]. The considerable annual production of these dyes, coupled with their frequent discharge into untreated effluents, underscores the urgent need to develop robust, sustainable methods to remove these and other organic pollutants from aquatic systems [6–8]. Global production of organic dyes and pigments is estimated at approximately 7 million tons per year, with over 12% reportedly lost to effluents during manufacturing and application processes [9,10]. Most of these compounds are inherently toxic and potentially carcinogenic, making their elimination from industrial wastewater an environmental challenge and reinforcing the need for effective decontamination strategies [11]. Among these dyes, methylene blue (MB) stands out as a representative pollutant because of its persistence, toxicity, and carcinogenic potential, posing significant risks to human health and aquatic ecosystems [12].

Researchers have investigated several technologies for removing refractory organic contaminants, including adsorption, biological degradation, and advanced oxidation processes (AOPs) [13,14]. Among these, AOPs have emerged as a promising route for degrading organic pollutants because they generate highly reactive, non-selective oxidizing species capable of mineralizing a broad spectrum of contaminants [15]. Heterogeneous photocatalysis, in particular, has garnered significant attention over the past two decades because it offers greater potential for industrial implementation than other AOPs. This technique effectively oxidizes a wide variety of organic molecules, such as dyes and pharmaceuticals [16]. The process involves photoactivating a semiconductor catalyst by exposing it to solar or artificial radiation (UV or visible), which promotes redox reactions on the catalyst surface [11]. These reactions generate reactive oxygen species, particularly hydroxyl radicals (•OH), which interact non-selectively with organic compounds and may ultimately mineralize them into stable end products such as $CO_2$ and $H_2O$ [17].

Selecting suitable catalysts with appropriate semiconducting properties is therefore essential. Niobium oxyhydroxide-based catalysts have recently attracted growing interest because of their strong performance in photocatalytic applications [18]. However, recovering these catalysts from aqueous media remains challenging. In many cases, the catalyst must be immobilized on a support material to facilitate solid–liquid separation [19]. Such support materials may serve multiple roles, including stabilizing the photocatalyst, enhancing contact with target pollutants, and improving recovery and reusability [20]. Common examples of support materials include glass, metals, and polymers [21,22]. Polymers offer an attractive alternative as catalyst supports because of their economic and practical advantages, especially biodegradable ones [23].

In heterogeneous photocatalysis, support materials can promote better catalyst dispersion, thereby enhancing catalytic activity. Increased surface area improves access to active sites, resulting in greater efficiency in degrading organic contaminants [21]. Moreover, supports can mitigate challenges such as catalyst nanoparticle agglomeration in aqueous media, which often complicates post-treatment separation [24]. Recent studies suggest that non-conjugated polymers lacking alternating single and double bonds can also serve as effective catalyst supports, opening new avenues in photocatalysis research [25]. These polymers, particularly biodegradable ones, are being explored because they are readily available, easy to process, and the final photocatalytic product may not require further post-treatment [26,27].

https://doi.org/10.3390/macromol6040116

Biodegradable polymers are a promising class of support materials because they are flexible, low-cost, chemically resistant, and environmentally compatible [28]. Polymers are among the most versatile functional materials, with tunable physicochemical, mechanical, and electronic properties [29]. Poly(butylene adipate-co-terephthalate) (PBAT) stands out in the field of sustainable materials for its combination of biodegradability and robust mechanical performance, alongside its ability to serve as a matrix for photocatalytic composites aimed at water remediation [30]. PBAT/PLA/$TiO_2$ composite films prepared via electrospinning have been used to degrade the dye Reactive Red BF-4B [31]. The membrane achieved 94.0% dye degradation within 24 h and was reused more than four times. Electrospinning was also used to obtain PBAT/PLA polymeric fibers combined with the semiconductors rutile titanium dioxide ($TiO_2$-R) and magnetite iron oxide ($Fe_3O_4$), aiming to degrade the dye Reactive Red 195, achieving 64.0% efficiency after 24 h [32]. These studies examined photocatalytic degradation of biodegradable composites and dyes, yielding promising results [31,32]. All the works mentioned above used PBAT/$TiO_2$, but they also incorporated other semiconductors or polymer blends, which may increase the final cost because more processing steps are required to obtain the final product.

In this context, the present study investigates the photocatalytic performance of biodegradable polyester-based composites containing niobium oxyhydroxide for degrading organic pollutants. Specifically, the objective was to evaluate the effectiveness of the PBAT polymer matrix as a support material for niobium oxyhydroxide, aiming to combine catalytic efficiency with environmental compatibility. The composites were prepared by melt extrusion, then hot-pressed, and characterized by Fourier-transform infrared spectroscopy (FTIR), thermogravimetric analysis (TGA), and differential scanning calorimetry (DSC) to assess structural, chemical, and thermal properties. Photocatalytic activity was evaluated by UV–Vis spectrophotometry under UV light irradiation using methylene blue as a model contaminant, while ESI(+)-MS analyses monitored degradation intermediates and elucidated the reaction mechanism.

## 2. Materials and Methods

### *2.1. Synthesis of Niobium Oxyhydroxide*

The synthesis of niobium oxyhydroxide (S2) was performed according to a previously reported procedure [33]. The same synthesis procedure was adopted in the present study. Therefore, this work focused on incorporating S2 into the PBAT matrix and evaluating the resulting composite materials. A total of 46.2 mmol of the precursor ammonium oxalate niobium salt ($NH_4NbO(C_2O_4)_2(H_2O)_n$), supplied by the Brazilian Company for Metallurgy and Mining (CBMM, Araxá, Brazil), was used. The niobium salt was dissolved in 100 mL of distilled water at 90 °C. After complete dissolution, $NH_4OH$, 5 mol/L (Synth, Diadema, Brazil) was slowly added until pH 7 was reached, promoting precipitation of niobium oxyhydroxide. The suspension was then stirred continuously for 12 h to age. Finally, the resulting white solid was filtered, washed, and dried in an oven at 60 °C for 12 h. To this material (300 mg), 4 mL of 30% hydrogen peroxide (Neon, Suzano, Brazil) and 80 mL of water at 25 °C were added. The resulting yellow solid was filtered, washed with distilled water, and dried at 60 °C for 12 h.

### *2.2. Preparation of Polymer/Catalyst Systems*

The PBAT/S2 composites were prepared using poly(butylene adipate-co-terephthalate) (PBAT-BASF (Ludwigshafen am Rhein, Germany)) in pellet form and niobium oxyhydroxide (S2). Three materials containing 0, 1, and 5 wt% S2 were prepared, corresponding to PBAT/S2 mass ratios of 100/0, 99/1, and 95/5, respectively, with a total

batch mass of 100 g. Thus, the reported S2 contents refer exclusively to the catalyst incorporated into the polymer matrix during melt processing. The mixtures were processed in a Thermo Scientific single-screw extruder (PolyLab 19/25 QC, Eindhoven, The Netherlands) at a screw speed of 50 rpm. Barrel temperatures were set to 100 °C in zones 1 and 4 and 120 °C in zones 2 and 3. The extrudates were subsequently pelletized using an AX-Plásticos pelletizer (ATX-50, Diadema, Brazil).

The resulting pellets were placed in a rectangular metallic mold cavity (150 × 100 × 1 mm), corresponding to a nominal film area of 150 $cm^2$ and a nominal thickness of 1 mm. The materials were compression-molded using an SL-11 hydraulic press (Solab, Piracicaba, Brazil) at 120 °C under a 4-metric-ton load for 3 min, then cooled to room temperature. For the surface-modified samples, 0.2 g of S2 was distributed over the film surface, corresponding to a nominal surface catalyst loading of approximately 1.33 $mg/cm^2$. This amount represents additional surface-deposited catalyst and is therefore reported separately from the S2 content (wt%) incorporated into the polymer matrix during extrusion.

To clearly distinguish the two catalyst incorporation strategies, samples containing S2 incorporated during extrusion are denoted PBAT/$S2_{1\%}$ and PBAT/$S2_{5\%}$. In contrast, samples additionally containing 0.2 g of surface-deposited S2 are identified by the suffix "$S2_{surf}$". Accordingly, the samples were designated PBAT, PBAT/$S2_{surf}$, PBAT/$S2_{1\%}$, PBAT/$S2_{1\%}$/$S2_{surf}$, PBAT/$S2_{5\%}$, and PBAT/$S2_{5\%}$/$S2_{surf}$, as summarized in Table 1.

**Table 1.** Nomenclature of each catalytic system and percentage of each raw material.

| Materials | PBAT (wt %) | Incorporated S2 (wt %) | Surface-Deposited S2 (g) | Catalyst Location |
|---|---|---|---|---|
| PBAT | 100 | 0 | - | - |
| PBAT/$S2_{surf}$ | 100 | 0 | 0.2 | Surface |
| PBAT/$S2_{1\%}$ | 99 | 1 | - | Matrix |
| PBAT/$S2_{1\%}$/$S2_{surf}$ | 99 | 1 | 0.2 | Matrix + surface |
| PBAT/$S2_{5\%}$ | 95 | 5 | - | Matrix |
| PBAT/$S2_{5\%}$/$S2_{surf}$ | 95 | 5 | 0.2 | Matrix + surface |

The PBAT and matrix-incorporated S2 contents are expressed as nominal weight percentages of the extruded formulations. For surface-modified films, 0.20 g of S2 was additionally deposited on-to the film surface and is reported separately from the matrix composition.

### *2.3. Materials Characterization*

Materials were characterized using Fourier transform infrared spectroscopy (FTIR) with an IR Prestige-21 (Shimadzu, Kyoto, Japan) equipped with an attenuated total reflectance (ATR) accessory. The following conditions were used: 64 scans over a spectral range of 4000–400 $cm^{-1}$. Thermogravimetric analysis (TG) was performed using a DTG-60 H (Shimadzu, Kyoto, Japan) with a flow rate of 50 mL $min^{-1}$ (under a synthetic $N_2$ atmosphere), a temperature range of 25 °C to 600 °C, and a heating rate of 10 °C · $min^{-1}$.

Differential scanning calorimetry (DSC) was performed using a DSC-60 instrument (Shimadzu). Samples were placed in aluminum pans and analyzed under a nitrogen atmosphere at a flow rate of 50 mL·$min^{-1}$. Two heating runs were carried out: (i) the first heating from 30 to 185 °C, with the final temperature held for 3 min, followed by cooling

down to –30 °C; (ii) the second heating from –30 °C to 190 °C. A constant heating/cooling rate of 10 °C·min$^{-1}$ was applied throughout all steps. The degree of crystallinity $X_c$ was calculated according to Equation (1).

$$X_c(\%) = \left[\frac{\Delta H_m}{W_{PBAT} \times \Delta H^\circ_m}\right] \times 100 \quad (1)$$

where $\Delta H_m$ is the experimental melting enthalpy, $W_{PBAT}$ is the PBAT mass fraction in the sample, and $\Delta H^\circ_m$ is the melting enthalpy of 100% crystalline PBAT (114 J/g).

Scanning electron microscopy (SEM) images of the external surfaces and fracture surfaces obtained after tensile testing were acquired using an SSX-550 (Shimadzu, Kyoto, Japan) instrument. The instrument's spatial resolution was 1.5 nm at 15 kV. Before SEM examination, the samples were sputter-coated with an approximately 20 nm thick gold layer.

### *2.4. Photocatalytic Activity and Dye Degradation Analysis*

Photocatalytic experiments were performed using 0.5 g of PBAT/S2 polymer films or 0.025 g of S2 powder, immersed in 15 mL of methylene blue (MB) solution (20 mg/L) at an initial pH of 7.2 and 22.5 °C. The experiments were conducted in a 60 × 50 cm reactor equipped with a UV lamp ($\lambda$ = 254 nm, nominal power = 15 W) positioned 40 cm from the reaction medium. The solution was stirred magnetically at 120 rpm. The experiments consisted of two consecutive stages: dark adsorption and photocatalysis. During the adsorption stage (−60 to 0 min), the UV lamp remained off, allowing MB molecules to interact with the catalytic materials. At t = 0 min, the UV lamp was turned on, initiating the photocatalytic stage, which continued for 120 min. Samples were collected at predetermined time intervals throughout both stages.

A photolysis control experiment was also performed using MB solution under UV irradiation (254 nm), without the catalyst or the polymeric film, under the same experimental conditions. MB concentration was monitored by UV–Vis spectrophotometry using a Bel spectrophotometer (model UV-M51, Monza, Italy) at 664 nm, corresponding to the characteristic MB absorption band. All experiments were performed in triplicate (n = 3).

Additionally, radical-scavenging experiments were performed using PBAT and PBAT/S2$_{5\%}$/S2$_{surf}$ to assess the contribution of hydroxyl radicals (·OH) to methylene blue degradation. Dimethyl sulfoxide (DMSO; Honeywell Specialty Chemicals, Seelze, Germany) served as the hydroxyl radical scavenger. A total of 1 mmol of DMSO was added to the reaction medium. These experiments evaluated the influence of HO• radicals on MB removal and provided further insight into the photocatalytic degradation mechanism.

All data were processed using OriginPro 9.8 software 2021 (OriginLab Corporation, Northampton, MA, USA). Methylene blue (MB) concentration was determined using a calibration curve. To construct the working analytical curve, methylene blue concentrations ranging from 10 to 35 mg/L were prepared by diluting an MB stock solution (35 mg/L) with distilled water. All photocatalytic experiments were performed in triplicate, and results are reported as the mean ± standard deviation. The degradation efficiency (%) was calculated for all experiments using spectrophotometric data according to the following equation (Equation (2)):

$$Remotion\ (\%) = \left(\frac{C_0 - C_t}{C_0}\right) \times 100 \quad (2)$$

where $C_0$ is the initial methylene blue concentration before the dark adsorption stage, and $C_t$ is the methylene blue concentration at reaction time *t*. The results were expressed as the percentage of removal (representing both adsorption and photocatalytic degradation), calculated from the pollutant concentration before and after treatment using Equation (2).

### *2.5. ESI-MS Spectrometry*

Possible intermediates, by-products, and structures of different species present in the product mixture were characterized using electrospray ionization-mass spectrometry (ESI-MS) with a mass spectrometer ION-TRAP LCQFleet (Thermo Fisher Scientific, San Jose, CA, USA) in positive polarity mode. The ESI(+)-MS analyses were performed under the following operating conditions: capillary temperature of 275 °C, nitrogen ($N_2$) as the nebulizing gas at a flow rate of 4 L $min^{-1}$, spray voltage of 2 kV, and tube lens offset of 25 V.

## 3. Results and Discussion

The FTIR spectra of PBAT, S2, and their mixtures are shown in Figure 1. The main absorption bands of PBAT, attributed to the asymmetric and symmetric stretching vibrations of $–CH_2$ groups, are observed at 2960 and 2873 $cm^{-1}$, corresponding to the C–H stretching of aliphatic groups in PBAT. The FTIR spectrum of PBAT exhibits intense absorption bands at 1715 $cm^{-1}$ associated with the carbonyl groups (C=O) in ester linkages. In the range of 1500 to 1000 $cm^{-1}$, absorption bands related to C=C stretching vibrations (νC=C) of aromatic rings present in the PBAT backbone are identified. Additionally, two prominent absorption bands, one broader and more intense than the other, are observed at 1267 and 1106 $cm^{-1}$. These are attributed to the stretching vibrations of the ester C–O bond (νC–O). The band around 800 $cm^{-1}$ corresponds to the out-of-plane deformation of the C–H bond in the phenylene ring [34,35].

The incorporation of the catalyst (S2) within the polymer matrix did not result in significant changes in the absorption bands associated with the polymer. This is expected because ATR is surface-sensitive, with a penetration depth limited to only a few micrometers. However, in samples where the catalyst was applied to the polymer surface, bands associated with the catalyst's OH groups were detected, as shown in Figure 1. The band observed at 3518 $cm^{-1}$ is attributed to the O–H stretching vibration associated with hydroxyl groups on the surface of the niobium oxyhydroxide catalyst, while the band at 3165 $cm^{-1}$ corresponds to the stretching of metal-bound hydroxyl groups (Nb–OH). The band at 3302 $cm^{-1}$ is related to the stretching vibration of O–H groups, which may originate either from the catalyst's structure or from adsorbed water on its surface [36,37].

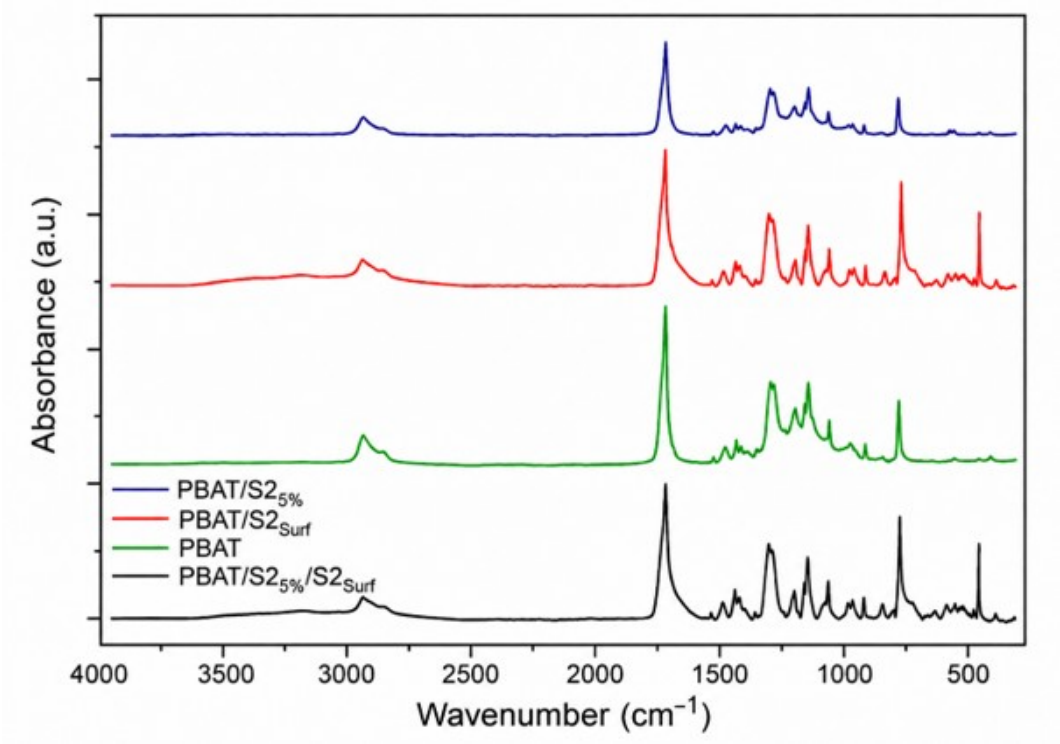



**Figure 1.** FTIR spectra of PBAT/S2$_{5\%}$, PBAT/S2$_{surf}$, PBAT/S2$_{5\%}$/S2$_{surf}$, and neat PBAT.

Finally, the band at 1710 cm$^{-1}$ shows lower relative intensity than in the pure PBAT spectrum. The reference bands of the polymer, such as that at 1260 cm$^{-1}$ in the FTIR spectrum of pure PBAT, appear shifted to 1270 cm$^{-1}$ in the spectra of Figure 1. The observed changes in the intensity and position of the C=O and C–O absorption bands suggest possible interfacial interactions between PBAT and S2. These spectral variations may arise from hydrogen bonding, coordination, dipole interactions, or changes in the local polymer environment. However, FTIR analysis alone cannot identify a specific interaction mechanism or confirm the formation of new chemical bonds.

For this study, FTIR vibrational spectroscopy proved a valuable tool for distinguishing compounds with catalysts on their surface from those without. Moreover, it enabled identification of interactions between the polymer and the catalyst, as shown by the bands in the spectrum in Figure 1, where the band at 850 cm$^{-1}$ is attributed to Nb–O stretching and to angular vibrations corresponding to Nb–O–Nb. Bands associated with niobium vibrations are also observed in the 500–700 cm$^{-1}$ region.

Scanning electron microscopy (SEM) coupled with energy-dispersive X-ray spectroscopy (EDS) was employed to investigate the morphology and elemental composition of the PBAT/S2$_{5\%}$/S2$_{surf}$ and PBAT/S2$_{5\%}$ composites, providing complementary information on the presence and spatial localization of the niobium-containing phase in the analyzed regions (Figure 2). The PBAT/S2$_{5\%}$/S2$_{surf}$ composite, containing both matrix-incorporated and additionally surface-deposited S2, exhibited a markedly heterogeneous surface morphology, with irregular regions and localized agglomerates (Figure 2A). EDS analyses performed on two morphologically distinct regions revealed differences in the relative intensities of the elemental signals. The brighter region (Region 1) exhibited more intense characteristic Nb signals, consistent with a Nb-enriched domain, whereas the darker region (Region 2) showed predominantly carbon and oxygen signals, along with weaker Nb signals (Figure 2A). These observations are consistent with differences in the local distribution of the niobium-containing phase, although the EDS spectra do not allow a quantitative assessment of its spatial distribution.

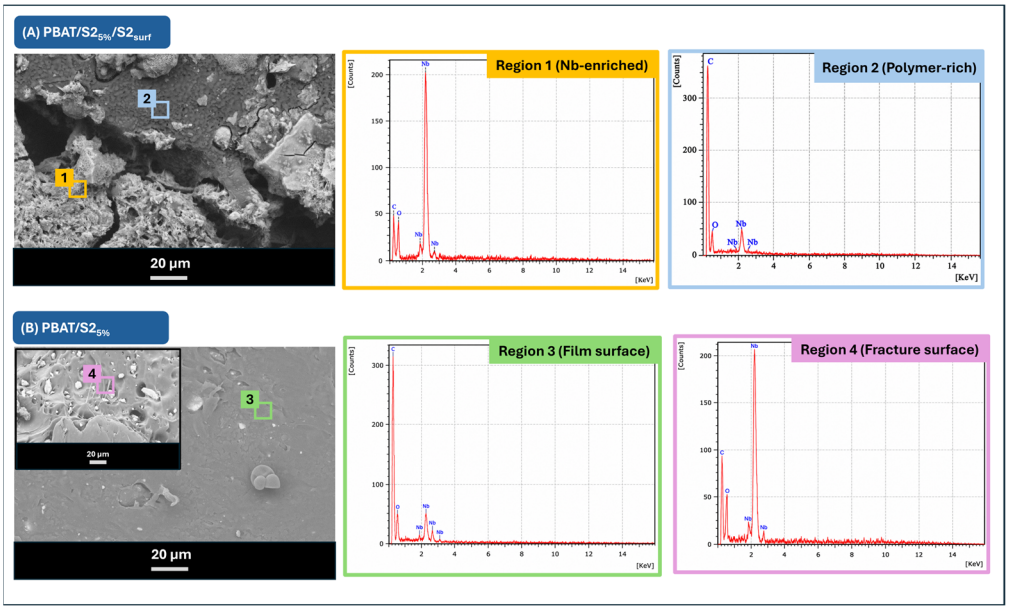



**Figure 2.** Scanning electron microscopy (SEM) images and corresponding energy-dispersive X-ray spectroscopy (EDS) spectra of PBAT/$NbO_2$(OH) composites prepared using different catalyst incorporation strategies. (**A**) PBAT/S2$_{5\%}$/S2$_{surf}$ composite containing matrix-incorporated and surface-deposited catalyst, showing (1) an Nb-enriched region and (2) a polymer-rich region. (**B**) PBAT/S2$_{5\%}$ composite containing catalyst incorporated by melt extrusion, showing EDS analyses of (3) the external film surface and (4) the fractured surface.

In contrast, the PBAT/S2$_{5\%}$ composite, in which S2 was incorporated into the polymer matrix during melt extrusion, exhibited a relatively continuous surface with localized irregularities, cavities, and particles of different sizes (Figure 2B). EDS analysis of the external film surface (Region 3) confirmed the presence of Nb, indicating that the niobium-containing phase was detectable at the surface despite being incorporated during processing. Examination of the fractured surface revealed a more irregular morphology, characterized by cavities, deformed polymeric regions, and dispersed particles. The corresponding EDS spectrum obtained from the fractured surface (Region 4) also showed characteristic Nb signals (Figure 2B), providing additional evidence of the presence of the niobium-containing phase within the polymeric material. These observations reveal morphological heterogeneity and confirm the presence of Nb in both the external and fractured regions of the composite.

The influence of niobium oxyhydroxide particle concentration on the thermal properties of PBAT was assessed using TGA (Figure 3). All samples displayed a single main degradation stage, characteristic of PBAT, associated with the decomposition of the aliphatic–aromatic polyester chains. The $T_{onset}$ and $T_{endset}$ temperatures showed no significant changes upon catalyst addition, indicating that niobium particles do not compromise the polymer's thermal stability.

At higher catalyst loadings, total mass loss decreased slightly, reaching approximately 85%. This reduction is consistent with the amount of inorganic phase incorporated and reflects its higher thermal stability. The higher residual mass observed above 500 °C for composites with greater S2 content is consistent with the presence of a thermally stable niobium-containing inorganic phase remaining after the main degradation stage of the PBAT matrix. The residual mass of the composites reflects contributions from both the PBAT matrix and the niobium-containing inorganic phase. Neat PBAT exhibited approximately 9% residual mass, which may be attributed to carbonaceous residues formed during thermal decomposition under a nitrogen atmosphere. PBAT/S2$_{5\%}$ and PBAT/S2$_{5\%}$/S2$_{surf}$ exhibited residual masses of approximately 12% and 14%, respectively. The higher

residual masses observed for the composites are consistent with the contribution of the niobium-containing inorganic phase, although possible interactions between the catalyst and the polymer matrix during thermal decomposition may also influence the final residue. Therefore, incorporating niobium oxyhydroxide particles into PBAT does not significantly alter the degradation mechanism, maintaining the polymer's processability and thermal resistance even in the presence of the catalyst.

The DSC curves obtained from the second heating and first cooling cycles (Figure 4 and Table S2 in the Supplementary Material) show the characteristic thermal events of PBAT and its nanocomposites. In the second heating cycle, an endothermic peak is observed, associated with the melting of PBAT's monoclinic ($\alpha$-form) crystalline phase, which is typical of this polymer. For PBAT/S2$_{5\%}$/S2$_{surf}$, PBAT/S2$_{5\%}$, PBAT/S2$_{surf}$, and PBAT/S2$_{1\%}$, the melting temperature ($T_m$) is essentially similar to that of pure PBAT, with only small variations ($\Delta T_m \leq 4$ °C), indicating that the incorporation of niobium oxyhydroxide nanoparticles does not significantly affect the crystalline structure responsible for the melting behavior of PBAT. Some DSC curves show a slight shoulder before the melting peak, consistent with crystal reorganization or perfection during heating. In the cooling curves, the exothermic crystallization peaks ($T_c$) appear between approximately 60 and 90 °C and shift with formulation and preparation method. This behavior suggests that, when well dispersed, the nanoparticles may influence the polymer's crystallization kinetics. In contrast, reductions in $T_c$ may indicate restricted chain mobility or a dilution effect in certain compositions. Overall, Tc variations are more sensitive to nanoparticle presence and dispersion than Tm variations.

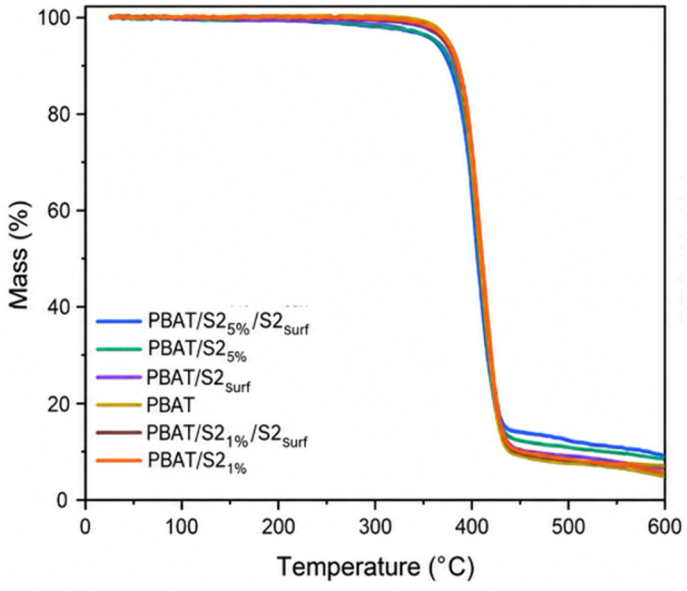



**Figure 3.** Thermogravimetric analysis TGA curve of neat PBAT and PBAT/S2$_{\%}$/S2$_{surf}$ nanocomposites obtained with different concentrations and preparation methods.

The degree of crystallinity ($X_c$) increased slightly with the addition of S2 nanoparticles, ranging from 7.9% to 11.1%, while the melting temperature decreased slightly. These results suggest that nanoparticles may modify the polymer's crystallization kinetics, thereby affecting molecular interactions within the matrix. Such effects can either facilitate or retard crystallization, depending on particle dispersion and concentration, consistent with previous studies [28,33,38]. These values are comparable to those reported in previous DSC studies of neat PBAT, including 10.2% reported by Khan et al. (2026) and approximately 15% reported in the literature for single-layer PBAT films [39].

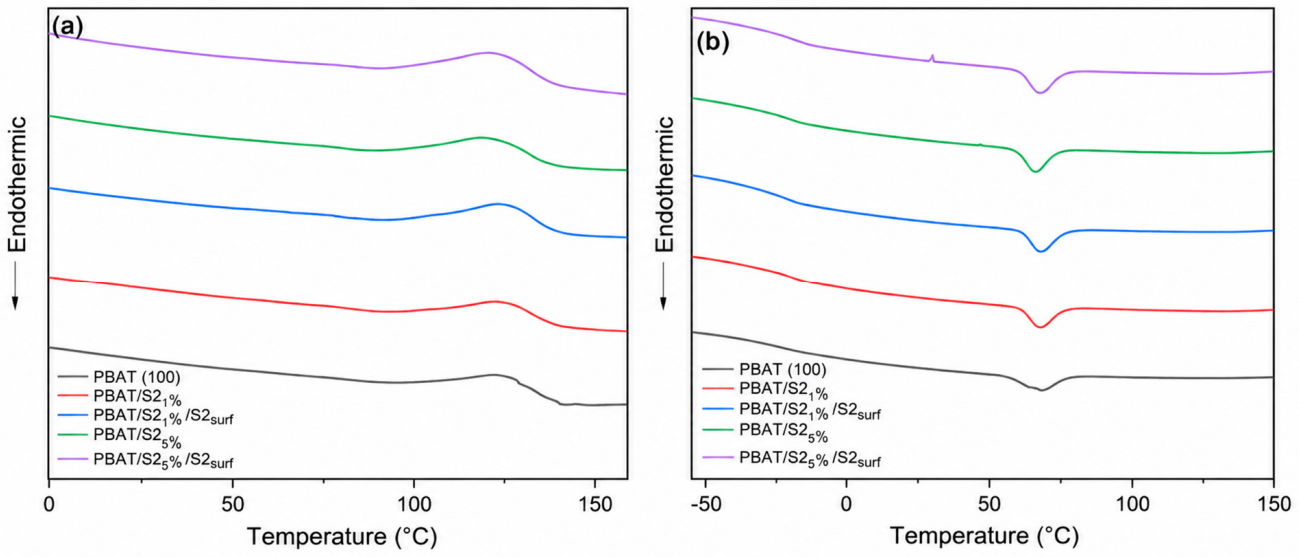



**Figure 4.** DSC curves of neat PBAT and PBAT/S2 composites obtained during the second (**a**) heating and (**b**) cooling cycles.

The kinetic curves for MB removal from aqueous solution in the presence of the catalytic systems under UV irradiation are presented in Figure 5. The photolysis control (MB), performed under UV irradiation without the catalyst or polymeric film, showed negligible changes in dye concentration throughout the experiment. This result indicates that direct photolysis contributed negligibly to methylene blue removal under the experimental conditions used. PBAT/niobium oxyhydroxide nanocomposite systems with different concentrations (0–5 wt%) achieved up to 88% total dye removal after 120 min of irradiation, whereas the dark process, predominantly dye adsorption, resulted in approximately 42% removal after 60 min. Incorporating the S2 catalyst into the polymer matrix enhanced methylene blue adsorption, regardless of the composite preparation method. The highest adsorption capacity was observed for PBAT/S2$_{5\%}$/S2$_{surf,}$ with about 42% removal, followed by PBAT/S2$_{1\%}$/S2$_{surf}$ with approximately 12%, while the neat polymer (PBAT) exhibited only ~4% adsorption. Notably, PBAT/S2$_{5\%}$, containing the catalyst only within the polymer matrix, exhibited approximately 8% adsorption, substantially lower than that observed for PBAT/S2$_{5}$%/S2$_{surf}$. These results suggest that the additional surface deposition of niobium oxyhydroxide favors methylene blue adsorption, potentially by increasing the accessibility of catalyst-containing regions at the film surface.

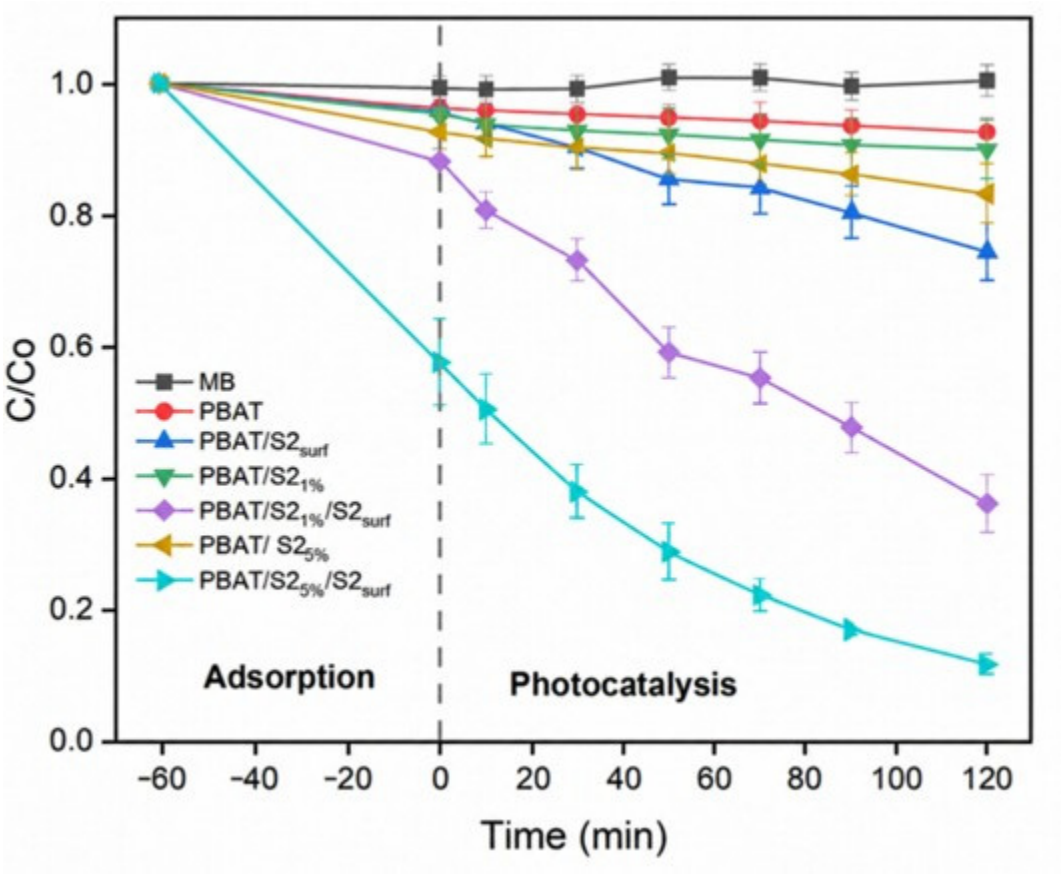



**Figure 5.** Methylene blue (MB) removal profiles obtained for the different PBAT/S2 catalytic systems during dark adsorption (−60 to 0 min) and UV irradiation (0 to 120 min). The curve labeled "MB" represents the photolysis control performed under UV irradiation without the catalyst or polymeric film.

The color changes observed in the PBAT/S2$_{5\%}$ films before and after photocatalysis (Figure S1 in the Supplementary Material) also visually confirm adsorption. Before the reaction, films containing higher catalyst loadings exhibited a slightly yellow hue, consistent with the intrinsic color of niobium oxyhydroxide. After the photocatalytic process, blue coloration increased progressively, particularly in films with higher catalyst content, indicating greater methylene blue adsorption.

Neat PBAT showed limited MB removal, with approximately 4% attributed to dark adsorption and an additional 3 percentage points of removal during UV irradiation, resulting in approximately 7% total dye removal after 120 min. This behavior is not expected to arise from conventional semiconductor-like electron–hole pair generation, since PBAT is a non-conjugated polymer and does not exhibit the typical electronic band structure of a semiconductor photocatalyst. According to Heitmann et al. (2019) [33], PBAT may undergo surface degradation under conditions involving UV irradiation and moisture, potentially involving radical-mediated photooxidative processes. Such processes could contribute to the limited dye removal observed for neat PBAT, although the specific reactive species responsible were not identified in the present study [40,41]. Therefore, while the polymer itself exhibits low dye removal activity, its use as a supporting matrix enables catalyst immobilization in a self-supporting film, facilitating handling and potential recovery from the aqueous medium.

Figure 6 shows how MB concentration changes over time in the presence of the PBAT/S2 film and its isolated precursors. The PBAT/S2$_{5\%}$/S2$_{surf}$ film achieved approximately 88% final dye removal, with about 42% attributed to adsorption, corresponding to

an adsorption uptake of 0.252 mg $g^{-1}$ of the composite film. The system containing only the S2 catalyst also exhibited high efficiency, with around 77% total dye removal, of which approximately 70% occurred during dark adsorption. These results indicate distinct removal profiles for the two systems. While adsorption predominated for isolated S2, the composite exhibited a greater additional reduction in MB concentration during UV irradiation. The superior performance of the PBAT/S2$_5$%/S2surf composite may suggest a synergistic contribution between the polymer matrix and S2, potentially associated with interfacial interactions and improved catalyst accessibility [40,41]. Furthermore, the self-supporting configuration of the composite facilitates catalyst handling and potential recovery from the aqueous medium, although its reusability and long-term operational stability remain to be experimentally evaluated [42,43].

To further investigate the contribution of reactive oxygen species to methylene blue removal, radical scavenging experiments were performed using dimethyl sulfoxide (DMSO), a commonly employed hydroxyl radical scavenger. As shown in Figure 6, the addition of DMSO markedly affected the removal performance of the PBAT/S2$_{5\%}$/S2$_{surf}$ composite. Without DMSO, the composite achieved approximately 88% methylene blue removal after 120 min of UV irradiation, whereas the removal decreased to approximately 53% in the presence of the scavenger. This reduction is consistent with the involvement of hydroxyl radicals (•OH) in the photoinduced degradation of methylene blue.

In contrast, neat PBAT showed only minor changes in methylene blue concentration, with or without DMSO, indicating that the polymer alone contributes little to dye removal under the conditions investigated. In the presence of S2, interfacial interactions between the polymer matrix and the catalyst may contribute to the photoinduced processes observed in the composite. As previously discussed, possible interfacial interactions between the carbonyl groups of PBAT and the hydroxylated surface of the niobium-based catalyst may influence the composite's behavior under UV irradiation. Nevertheless, the present experiments do not provide direct evidence of PBAT's specific role in these interfacial processes. The persistence of dye removal in the presence of DMSO indicates that the overall process cannot be attributed exclusively to DMSO-sensitive radical pathways. Initial adsorption, residual photoinduced activity, and other possible reaction pathways may contribute to the observed performance. Furthermore, the non-monotonic concentration profile observed in the presence of DMSO suggests that additional processes, including changes in adsorption–desorption behavior, may influence the measured dye concentration. Therefore, the scavenging results provide indirect evidence supporting the participation of hydroxyl radicals.

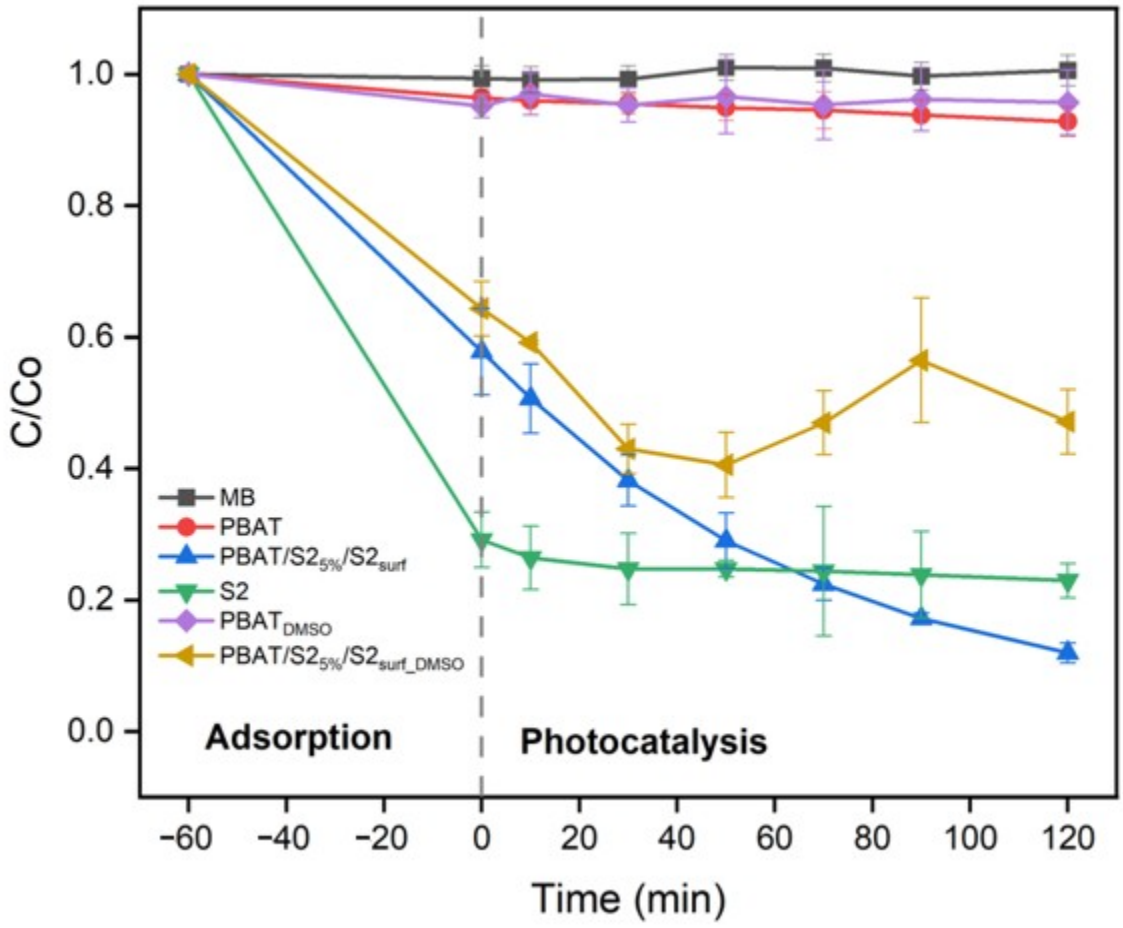



**Figure 6.** Kinetic curves of MB removal evaluating the individual contributions of PBAT and S2, including hydroxyl radical scavenging experiments performed with PBAT and PBAT/S2$_{5\%}$/S2$_{surf}$ in the presence of DMSO.

The photocatalytic performance of the PBAT/S2$_{5\%}$/S2$_{surf}$ system is consistent with the efficiencies reported for other supported and immobilized photocatalytic materials (Table 2). Rizzo et al. (2007) reported approximately 80% methylene blue removal using a $TiO_2$ nanofilm immobilized on a polymethylmethacrylate (PMMA) reactor under UV irradiation, demonstrating the feasibility of polymer-supported photocatalysts for water treatment [44]. Similarly, $TiO_2$ immobilized on a polystyrene membrane resulted in approximately 68% methylene blue degradation after 5 h of solar irradiation [45]. $TiO_2$ supported on a ceramic material achieved approximately 60–70% degradation under UVC irradiation [46]. Regarding niobium-based photocatalysts, supported $Nb_2O_5$ systems have been reported to achieve nearly complete methylene blue degradation after 3 h of sunlight exposure [47]. These comparisons should be interpreted cautiously because photocatalytic efficiency strongly depends on experimental conditions, including irradiation source, catalyst loading, initial dye concentration, pH, and reactor configuration. Nevertheless, the approximately 88% removal obtained in the present study indicates that immobilization of S2 on PBAT preserves relevant photocatalytic activity while providing a readily recoverable solid photocatalytic system.

**Table 2.** Comparison of photocatalytic systems reported in the literature and obtained in the present study.

| System | Radiation Source | Catalyst Content | Reaction Conditions | Removal Efficiency | Ref. |
|---|---|---|---|---|---|
| $TiO_2$ nanofilm immobilized on PMMA rings | UV | $TiO_2$ (5.8 g/L) sprayed onto the rings (0.011 mL/cm$^2$) | 10 min | 80% | [44] |
| Heterogeneous $TiO_2$ suspension | High-pressure Hg lamp: $\lambda \geq 290$ nm and $\lambda \geq 340$ nm | 2.5 g/L | 60 min ($\lambda \geq 290$ nm) to 120 min ($\lambda \geq 340$ nm) | 100% decolorization and degradation. | [24] |
| Niobium oxyhydroxide incorporated into PHB film | UV-Vis | 5 wt% niobium oxyhydroxide in the PHB matrix | 120 min | 90–96% | [38] |
| Niobium- and nitrogen-co-doped $TiO_2$ | Sunlight | 0.64 g/L | 105 min | 98,50% | [37] |
| $TiO_2$ immobilized on a polystyrene membrane | Sunlight | 4% $TiO_2$ in the membrane casting solution | 300 min | 68% | [45] |
| $TiO_2$ supported on porous ceramics | UVC | 0.4 g/50 g | 60 min | 60–70% | [46] |
| Niobium oxyhydroxide incorporated into PHB, PP, and WPU polymer matrices | UV | 2% $NbO_2(OH)$ in the polymer matrix | 60 min to 90 min | 90%-PHB and 60 min; 80% WPU; 40%-PP and 90 min | [33] |
| Niobium oxyhydroxide incorporated into PBAT | UV | 5 wt% $NbO_2(OH)$ incorporated into the PBAT matrix, with an additional 0.2 g deposited on the surface | 120 min | 88% | This Study |

ESI(+)-MS monitored MB degradation by the catalytic system containing a niobium-based catalyst incorporated into PBAT. The ESI(+)-MS spectrum of the initial solution showed an intense signal at *m*/*z* 284, assigned to MB, along with signals at *m*/*z* 347 and 205, attributed to column impurities (Figure 7). After 30 min of reaction, a decrease in the intensity of the MB signal was observed, accompanied by the appearance of new ions at *m*/*z* 281 and 223. In contrast, the signals at *m*/*z* 347 and 205 remained essentially unchanged. After 2 h of photocatalytic reaction, additional ions emerged, together with a pronounced decrease in the relative intensity of the characteristic MB signal at *m*/*z* 284. Based on the most intense *m*/*z* signals, a degradation pathway involving hydroxyl radicals (•OH) was proposed (Figure 7), providing evidence of the progressive oxidation and fragmentation of the MB molecule. Overall, these results indicate that the photocatalytic process promotes extensive MB degradation, reaching an advanced oxidation stage before complete mineralization.

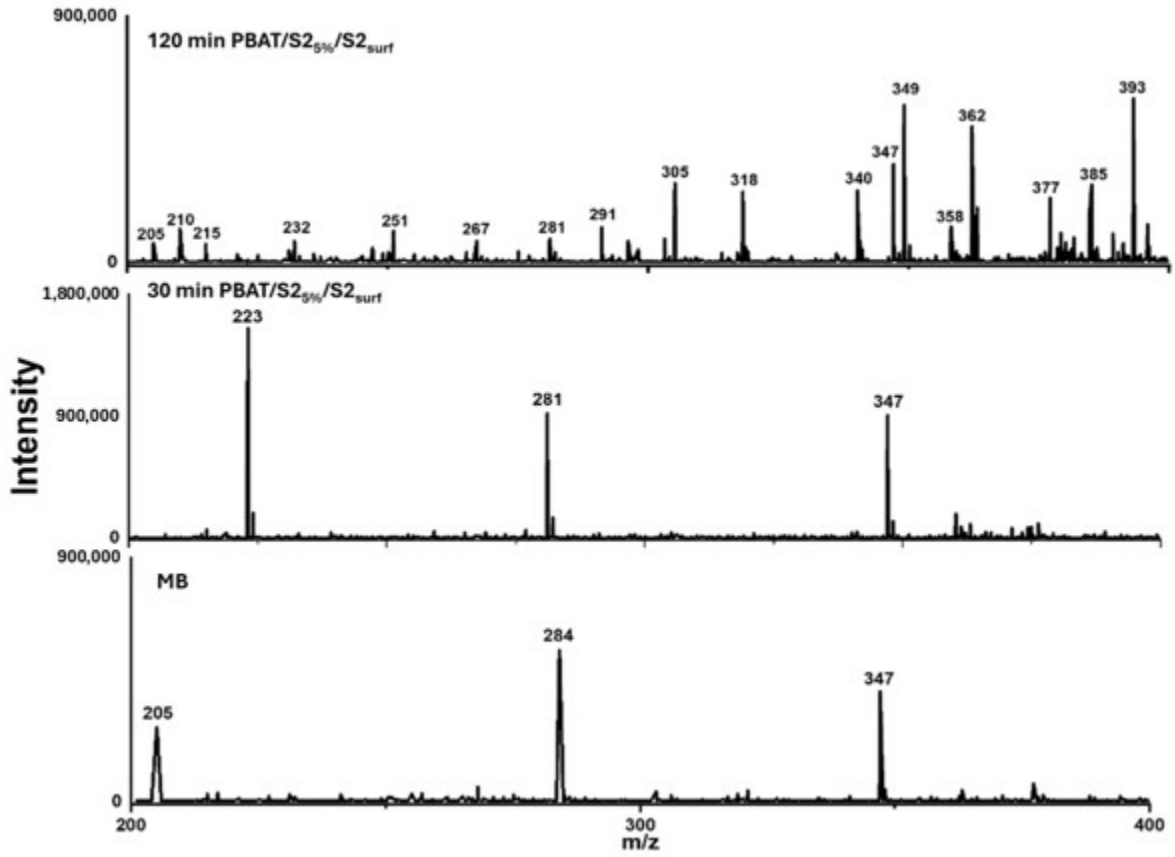



**Figure 7.** ESI(+)-MS spectra of the MB standard solution using the PBAT/S2$_{5\%}$/S2$_{surf}$ catalyst under UV irradiation after 30 and 120 min of the photocatalytic reaction.

The methylene blue removal process involves two distinct but complementary stages: initial adsorption of dye molecules onto the polymer/catalyst surface and subsequent photocatalytic oxidation under UV irradiation. The PBAT/S2$_{5\%}$/S2$_{surf}$ system exhibited the highest adsorption capacity, consistent with the greater availability of hydroxylated sites (Nb–OH) at the interface. Similar behavior has been reported for $Nb_2O_5$-based composites, where surface hydroxyl groups anchor dye molecules through electrostatic interactions and enhance photoinduced charge transfer [25,38]. When UV irradiation begins, photoexcited electrons in S2 migrate to the conduction band, generating holes ($h^+$) in the valence band that react with adsorbed $H_2O$ to produce highly reactive hydroxyl radicals (•OH). These radicals initiate oxidation and ring-opening of the methylene blue molecule, a pathway corroborated by the ions detected in the ESI(+)-MS (*m*/*z* 274, 362, and 394) [24]. The detected ions were tentatively assigned based on their nominal *m*/*z* values and previously reported MB degradation pathways. Since MS/MS or high-resolution mass spectrometry was not performed, these assignments should be considered tentative rather than definitive structural identifications.

These chemical modifications increase the surface hydrophilicity and introduce polar –COO and -OH groups, which favor the adsorption of methylene blue molecules through electrostatic interactions. In parallel, localized formation of •OH species during the photo-assisted cleavage contributes to the oxidative degradation and ring opening of methylene blue, as evidenced by the ions detected in the ESI(+)-MS at *m*/*z* 394, 362, 318, 301, 281, 223, and 274 (Figure 8). Therefore, partial oxidation of the PBAT matrix not only improves dye adsorption and charge separation but also generates reactive oxygen species that accelerate photocatalytic degradation.

Beyond serving as support, the polymer matrix plays an active role in the overall photocatalytic behavior. In the presence of a photocatalyst, biodegradable polyesters such

as PBAT can undergo superficial photo-oxidation under UV exposure, generating a small quantity of •OH radicals through chain scission and carbonyl-group oxidation [25]. This phenomenon may partially account for the slight degradation observed in neat PBAT and may contribute synergistically to the photocatalytic process in the composites. Furthermore, the polarity of the PBAT chains may favor interactions with S2, contributing to improved particle dispersion and interfacial adhesion. This interpretation is supported by the shifts observed in the FTIR bands associated with the C=O and C–O groups. This structural compatibility facilitates electron transfer between the polymer and the catalyst surface, reducing recombination and enhancing the effective lifetime of photogenerated carriers.

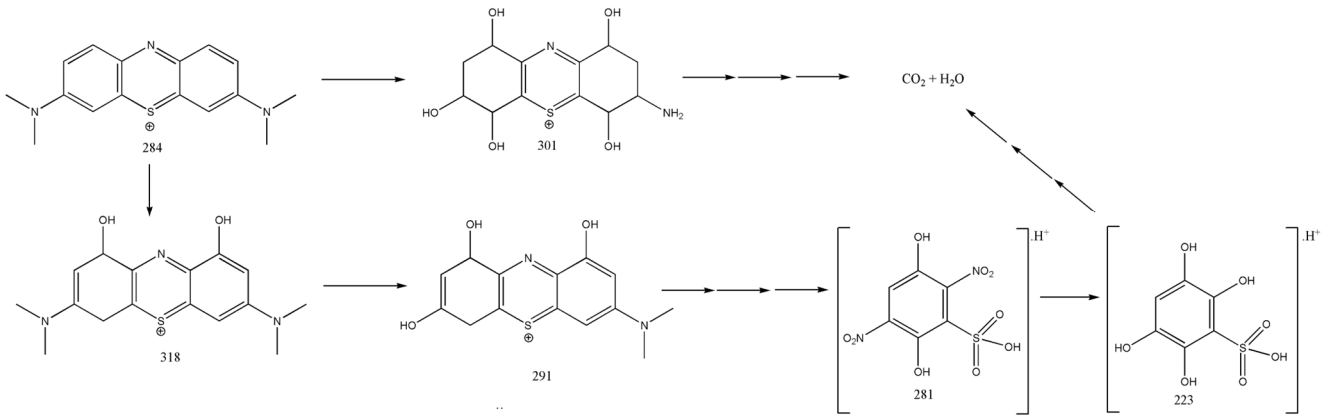



**Figure 8.** Proposed mechanism for the photo-assisted hydrolytic degradation of the MB standard solution using the PBAT/S2$_{5\%}$/S2$_{surf}$ catalyst under UV irradiation after 30 and 120 min of the photocatalytic reaction.

The ESI-MS analysis of the aqueous phase did not provide direct evidence of degradation products that could be unequivocally attributed to PBAT. Therefore, although photo-assisted transformations at the PBAT/S2 interface may occur under UV irradiation, the proposed PBAT degradation pathway should be regarded as a mechanistic hypothesis rather than an experimentally confirmed reaction pathway. In addition to the photocatalytic degradation of methylene blue, a possible photo-assisted interfacial pathway involving PBAT and S2 is proposed, as illustrated in Figure 9. In this hypothesis, interactions at the polymer–catalyst interface may facilitate proton-coupled electron transfer (PCET) processes and promote hydrolytic reactions involving PBAT ester groups. However, the present study provides no direct experimental evidence for PCET, so this pathway should be regarded as a proposed mechanism rather than a validated reaction route. Further spectroscopic and mechanistic investigations are required to confirm this hypothesis.

However, the present study did not obtain direct experimental evidence for this PCET-mediated pathway. Therefore, the mechanism shown in Figure 9 should be considered a hypothesis that requires further experimental validation. The present results demonstrate MB removal and the formation of transformation products, but do not demonstrate complete mineralization. Since TOC or COD analyses were not performed, the extent of mineralization could not be determined.

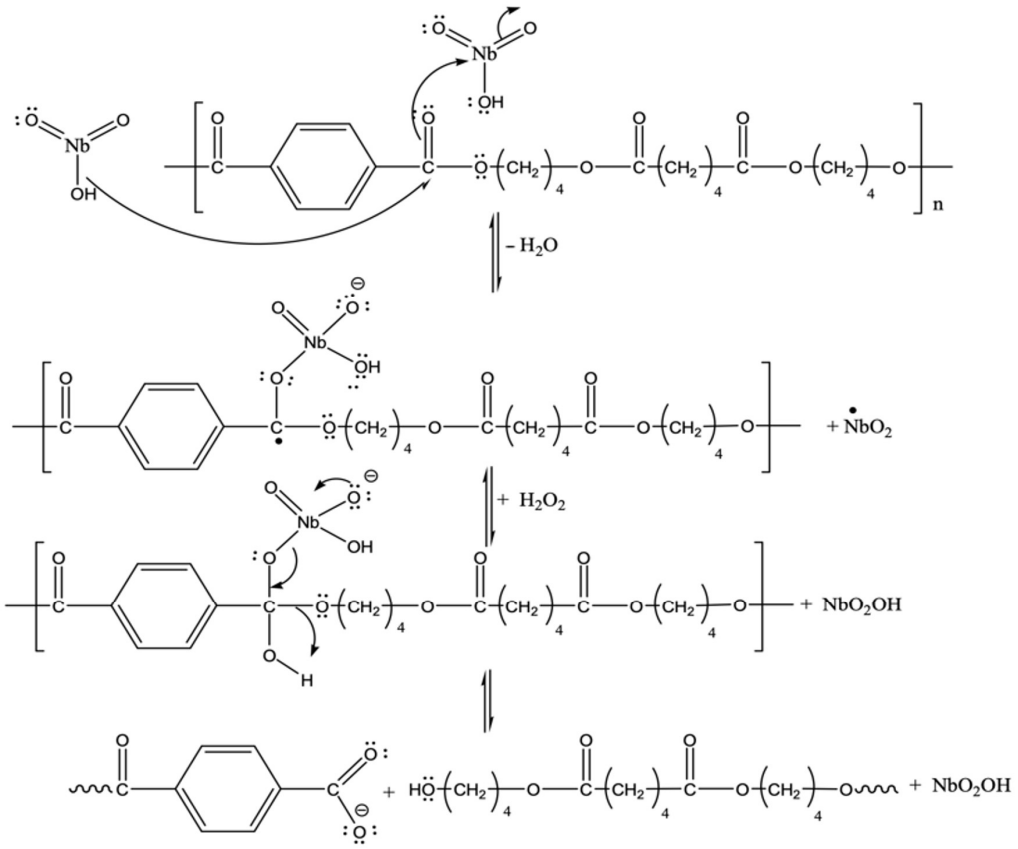



**Figure 9.** Hypothetical photo-assisted hydrolytic pathway of PBAT at the interface with $NbO_2(OH)$, involving a possible PCET process.

## 4. Conclusions

The PBAT/S2 composites developed in this study demonstrated promising potential as self-supporting materials for methylene blue removal from aqueous media under UV irradiation. FTIR analysis suggested possible interfacial interactions between PBAT and S2, as indicated by changes in the position and intensity of characteristic polymer bands. DSC and TGA results showed that S2 did not significantly alter PBAT's thermal properties, preserving the composites' processability.

Incorporating S2 into the PBAT matrix, combined with additional catalyst deposition on the film surface, resulted in the highest methylene blue removal among the investigated formulations. The PBAT/$S2_{5\%}$/$S2_{surf}$ composite, containing 5 wt% S2 incorporated into the polymer matrix and an additional 0.2 g of S2 deposited on the surface, achieved approximately 88% total dye removal, comprising 42% during dark adsorption and an additional 46 percentage points during 120 min of UV irradiation. Scavenging experiments using DMSO reduced total dye removal to approximately 53%, supporting the involvement of DMSO-sensitive photoinduced pathways, including those potentially mediated by hydroxyl radicals.

From the ESI-MS spectrum, it is possible to observe *m*/*z* signals of molecules consistent with oxidative degradation and ring opening of MB. From an application standpoint, developing polymer-supported photocatalysts addresses one of the main bottlenecks in advanced oxidation processes: catalyst recovery. The PBAT/S2 films combine high removal efficiency with mechanical integrity, enabling recovery of the catalyst after the photocatalytic process. Therefore, immobilizing niobium oxyhydroxide on a

biodegradable matrix not only improves environmental compatibility but also supports operational sustainability in wastewater remediation.

From an application perspective, immobilizing S2 in a self-supporting PBAT film offers a practical advantage over dispersed catalyst powders by facilitating material handling and potential recovery from aqueous media. Overall, the results demonstrate the potential of PBAT/S2 composites as immobilized catalytic systems for dye removal, while further studies on catalyst stability, reusability, and the contribution of polymer–catalyst interfacial processes are needed to assess their long-term performance.

**Supplementary Materials:** The following supporting information can be downloaded at https://www.mdpi.com/article/10.3390/macromol6040116/s1: Table S1. Thermal analysis parameters of pure PBAT and PBAT/S2 composites obtained from TGA-curve; Table S2. Thermal properties obtained from the DSC curves of the second heating and first cooling cycles for pure PBAT and PBAT/S2 nanocomposites; Figure S1. Visual appearance of PBAT/S2 films prepared with different catalyst concentrations before (A) and after (B–H) the photocatalytic reaction under UV irradiation. Higher catalyst content yields more pronounced yellow coloration before the reaction and deeper blue coloration after photocatalysis, consistent with catalyst distribution and methylene blue adsorption.

**Author Contributions:** M.E.S.P.: Data curation, Methodology, Validation, and Formal analysis—Writing—original draft & editing. A.P.H.: Conceptualization, Project administration, Supervision and Writing—original draft & editing. L.C.M.: Investigation, Formal analysis and Validation. I.B.: Validation and Writing—original draft & editing. R.A.: Validation and Writing—original draft & editing. E.F.P.: Investigation and Formal analysis. J.B.d.O.: Conceptualization and Writing—original draft & editing. P.P.d.S.: Conceptualization, Resources; Writing—review & editing. L.C.A.d.O.: Methodology, Resources; Supervision; Writing—review & editing. P.S.d.O.P.: Conceptualization, Resources; Project administration, Supervision, and Writing—review & editing. All authors have read and agreed to the published version of the manuscript.

**Funding:** The APC was funded by CAPES-PROAP.

**Data Availability Statement:** The original contributions presented in this study are included in the article/Supplementary Material. Further inquiries can be directed to the corresponding author(s).

**Acknowledgments:** The authors thank the Coordenação de Aperfeiçoamento de Pessoal de Nível Superior—Brasil (CAPES)-Code 001, Fundação de Amparo à Pesquisa do Estado de Minas Gerais (FAPEMIG-APQ-03705-23), INCTNb - Inovação em Processos e Produtos Baseados em Nióbio (CNPq 408482/2024-9) and the National Council for Scientific and Technological Development (CNPq).

**Conflicts of Interest:** The authors declare no conflicts of interest.

## References

1. Oller, I.; Malato, S.; Sánchez-Pérez, J.A. Combination of Advanced Oxidation Processes and Biological Treatments for Wastewater Decontamination-A Review. *Sci. Total Environ.* **2011**, *409*, 4141–4166. https://doi.org/10.1016/j.scitotenv.2010.08.061.
2. Moradi, S.; Babapoor, A.; Ghanbarlou, S.; Kalashgarani, M.Y.; Salahshoori, I.; Seyfaee, A. Toward a New Generation of Fertilizers with the Approach of Controlled-Release Fertilizers: A Review. *J. Coat. Technol. Res.* **2024**, *21*, 31–54. https://doi.org/10.1007/s11998-023-00817-z.
3. Tkaczyk, A.; Mitrowska, K.; Posyniak, A. Synthetic Organic Dyes as Contaminants of the Aquatic Environment and Their Implications for Ecosystems: A Review. *Sci. Total Environ.* **2020**, *717*, 137222. https://doi.org/10.1016/j.scitotenv.2020.137222.
4. Lu, J.; Zhang, H.; Li, S.; Guo, S.; Shen, L.; Zhou, T.; Zhong, H.; Wu, L.; Meng, Q.; Zhang, Y. Oxygen-Vacancy-Enhanced Peroxidase-like Activity of Reduced $Co_3O_4$ Nanocomposites for the Colorimetric Detection of $H_2O_2$ and Glucose. *Inorg. Chem.* **2020**, *59*, 3152–3159. https://doi.org/10.1021/acs.inorgchem.9b03512.

5. Zuo, C.; Tai, X.; Jiang, Z.; Liu, M.; Jiang, J.; Su, Q.; Yan, X. S-Scheme 2D/2D Heterojunction of $ZnTiO_3$ Nanosheets/$Bi_2WO_6$ Nanosheets with Enhanced Photoelectrocatalytic Activity for Phenol Wastewater under Visible Light. *Molecules* **2023**, *28*, 3495. https://doi.org/10.3390/molecules28083495.
6. Kusumlata; Ambade, B.; Kumar, A.; Gautam, S. Sustainable Solutions: Reviewing the Future of Textile Dye Contaminant Removal with Emerging Biological Treatments. *Limnol. Rev.* **2024**, *24*, 126–149. https://doi.org/10.3390/limnolrev24020007.
7. Cui, Y.; Chen, Y.; Cao, Z.; Xu, L.; He, J.; Zhu, Z.; Lian, L.; Luo, X.; Yang, Z.; Chen, M. Oxidation of Toluene over the Pt-Embedded Mesoporous $CeO_2$ Hollow Nanospheres with Advanced Catalytic Performances. *Inorg. Chem.* **2024**, *63*, 19972–19990. https://doi.org/10.1021/acs.inorgchem.4c03562.
8. Pan, X.; Ji, J.; Zhang, N.; Xing, M. Research Progress of Graphene-Based Nanomaterials for the Environmental Remediation. *Chinese Chem. Lett.* **2020**, *31*, 1462–1473. https://doi.org/10.1016/j.cclet.2019.10.002.
9. Rauf, M.A.; Ashraf, S.S. Fundamental Principles and Application of Heterogeneous Photocatalytic Degradation of Dyes in Solution. *Chem. Eng. J.* **2009**, *151*, 10–18. https://doi.org/10.1016/j.cej.2009.02.026.
10. Kapanga, P.M.; Nyakairu, G.W.A.; Nkanga, C.I.; Lusamba, S.N.; Tshimanga, R.M.; Shehu, Z. A Review of Dye Effluents Polluting African Surface Water: Sources, Impacts, Physicochemical Properties, and Treatment Methods. *Discov. Water* **2024**, *4*, 85. https://doi.org/10.1007/s43832-024-00129-2.
11. Tian, D.; Zhou, H.; Zhang, H.; Zhou, P.; You, J.; Yao, G.; Pan, Z.; Liu, Y.; Lai, B. Heterogeneous Photocatalyst-Driven Persulfate Activation Process under Visible Light Irradiation: From Basic Catalyst Design Principles to Novel Enhancement Strategies. *Chem. Eng. J.* **2022**, *428*, 131166. https://doi.org/10.1016/j.cej.2021.131166.
12. Ahmadi, B.; Fallah, A.; Ghamarpoor, R.; Jamshidi, M. Methylene Blue beyond the Dye: A Critical Review on Its Role as a Benchmark Pollutant in Photocatalyst Design. *Results Chem.* **2025**, *18*, 102910. https://doi.org/10.1016/j.rechem.2025.102910.
13. Akerdi, A.G.; Bahrami, S.H. Application of Heterogeneous Nano-Semiconductors for Photocatalytic Advanced Oxidation of Organic Compounds: A Review. *J. Environ. Chem. Eng.* **2019**, *7*, 103283. https://doi.org/10.1016/j.jece.2019.103283.
14. Pang, Y.L.; Abdullah, A.Z. Current Status of Textile Industry Wastewater Management and Research Progress in Malaysia: A Review. *CLEAN Soil Air Water* **2013**, *41*, 751–764. https://doi.org/10.1002/clen.201000318.
15. Pandis, P.K.; Kalogirou, C.; Kanellou, E.; Vaitsis, C.; Savvidou, M.G.; Sourkouni, G.; Zorpas, A.A.; Argirusis, C. Key Points of Advanced Oxidation Processes (AOPs) for Wastewater, Organic Pollutants and Pharmaceutical Waste Treatment: A Mini Review. *ChemEngineering* **2022**, *6*, 8. https://doi.org/10.3390/chemengineering6010008.
16. Oviedo, L.R.; Muraro, P.C.L.; Pavoski, G.; Espinosa, D.C.R.; Ruiz, Y.P.M.; Galembeck, A.; Rhoden, C.R.B.; da Silva, W.L. Synthesis and Characterization of Nanozeolite from (Agro)Industrial Waste for Application in Heterogeneous Photocatalysis. *Environ. Sci. Pollut. Res.* **2022**, *29*, 3794–3807.
17. Chen, H.Y. Why the Reactive Oxygen Species of the Fenton Reaction Switches from Oxoiron(IV) Species to Hydroxyl Radical in Phosphate Buffer Solutions? A Computational Rationale. *ACS Omega* **2019**, *4*, 14105–14113. https://doi.org/10.1021/acsomega.9b02023.
18. Fidelis, M.Z.; Faria, J.; Santacruz, W.; Lima, T.S.; Lenzi, G.G.; Motheo, A.J. Niobium-Based Catalysts in Advanced Oxidation Processes: A Systematic Review of Mechanisms, Material Engineering, and Environmental Applications. *Environments* **2025**, *12*, 311. https://doi.org/10.3390/environments12090311.
19. Luckachan, G.E.; Pillai, C.K.S. Biodegradable Polymers- A Review on Recent Trends and Emerging Perspectives. *J. Polym. Environ.* **2011**, *19*, 637–676. https://doi.org/10.1007/s10924-011-0317-1.
20. Ainali, N.M.; Bikiaris, D.N.; Lambropoulou, D.A. Aging Effects on Low- and High-Density Polyethylene, Polypropylene and Polystyrene under UV Irradiation: An Insight into Decomposition Mechanism by Py-GC/MS for Microplastic Analysis. *J. Anal. Appl. Pyrolysis* **2021**, *158*, 105207. https://doi.org/10.1016/j.jaap.2021.105207.
21. Wei, Z.-Q.; Hou, S.; Lin, X.; Xu, S.; Dai, X.-C.; Li, Y.-H.; Li, J.-Y.; Xiao, F.-X.; Xu, Y.-J. Unexpected Boosted Solar Water Oxidation by Nonconjugated Polymer-Mediated Tandem Charge Transfer. *J. Am. Chem. Soc.* **2020**, *142*, 21899–21912. https://doi.org/10.1021/jacs.0c11057.
22. He, X.; Zhang, F.; Li, C.; Ding, W.; Jin, Y.; Tang, L.; Huang, R. Effect of Starch Plasticization on Morphological, Mechanical, Crystalline, Thermal, and Optical Behavior of Poly(butylene adipate-co-terephthalate)/Thermoplastic Starch Composite Films. *Polymers* **2024**, *16*, 326.
23. Ainali, N.M.; Kalaronis, D.; Evgenidou, E.; Bikiaris, D.N.; Lambropoulou, D.A. Insights into Biodegradable Polymer-Supported Titanium Dioxide Photocatalysts for Environmental Remediation. *Macromol* **2021**, *1*, 201–233. https://doi.org/10.3390/macromol1030015.

24. Houas, A.; Lachheb, H.; Ksibi, M.; Elaloui, E.; Guillard, C.; Herrmann, J.M. Photocatalytic Degradation Pathway of Methylene Blue in Water. *Appl. Catal. B Environ.* **2001**, *31*, 145–157. https://doi.org/10.1016/S0926-3373(00)00276-9.
25. Heitmann, A.P.; Coura Rocha, I.; de Souza, P.P.; Oliveira, L.C.A.; Patrícia, P.S. Photoactivation of a Biodegradable Polymer (PHB): Generation of Radicals for Pollutants Oxidation. *Catal. Today* **2020**, *344*, 171–175. https://doi.org/10.1016/j.cattod.2018.12.024.
26. Natarajan, S.; Bajaj, H.C.; Tayade, R.J. Recent Advances Based on the Synergetic Effect of Adsorption for Removal of Dyes from Waste Water Using Photocatalytic Process. *J. Environ. Sci.* **2018**, *65*, 201–222. https://doi.org/10.1016/j.jes.2017.03.011.
27. Kant, R. Textile Dyeing Industry an Environmental Hazard. *Nat. Sci.* **2012**, *04*, 22–26. https://doi.org/10.4236/ns.2012.41004.
28. Jian, J.; Xiangbin, Z.; Xianbo, H. An Overview on Synthesis, Properties and Applications of Poly(Butylene-Adipate-Co-Terephthalate)—PBAT. *Adv. Ind. Eng. Polym. Res.* **2020**, *3*, 19–26. https://doi.org/10.1016/j.aiepr.2020.01.001.
29. Dhas, P.G.T.N.; Gulyas, H.; Otterpohl, R. Impact of Powdered Activated Carbon and Anion Exchange Resin on Photocatalytic Treatment of Textile Wastewater. *J. Environ. Prot.* **2015**, *06*, 191–203. https://doi.org/10.4236/jep.2015.63020.
30. Matusinho, I.A. do. S.; Ramos, T.F.; de Oliveira, J.B.; Pedroso, E.F.; de Souza, P.P.; Patricio, P.S. d. O. Influence of Starch Source on Properties of Blends Based on Thermoplastic Starch and Poly(Butylene-Adipate-Co-Terephthalate). *Carbohydr. Polym. Technol. Appl.* **2024**, *7*, 100433. https://doi.org/10.1016/j.carpta.2024.100433.
31. Rosenberger, A.G.; Ballmann, E.; Lima, F. da S.; Caetano, J.; Dragunski, D.C.; Muniz, E.C.; Módenes, A.N. Electrospun Polymeric Film in Red BF-4B Dye Degradation. *Polymers* **2025**, *17*, 2669. https://doi.org/10.3390/polym17192669.
32. Medeiros, A.R.; Lima, S.; Rosenberger, A.G.; Dragunski, D.C.; Muniz, E.C.; Radovanovic, E.; Caetano, J. Poly(butylene adipate-co-terephthalate)/Poly(lactic acid) Polymeric Blends Electrospun with $TiO_2$-R/$Fe_3O_4$ for Pollutant Photodegradation. *Polymers* **2023**, *15*, 762.
33. Heitmann, A.P.; Rocha, I.C.; Pereira, I.M.; Oliveira, L.C.A.; de Oliveira Patrício, P.S. Nanoparticles of Niobium Oxyhydroxide Incorporated in Different Polymers for Photocatalytic Degradation of Dye. *J. Polym. Res.* **2019**, *26*, 159. https://doi.org/10.1007/s10965-019-1824-3.
34. Niksefat, M.; Bagheri, R.; Pourjavadi, A. Biodegradable PBAT Films with in Situ Synthesized Tannic Acid/ZnS Nanohybrids for Active Packaging, Offering Antioxidant, Antibacterial, and UV-Shielding Properties. *Sci. Rep.* **2026**, *16*, 1198. https://doi.org/10.1038/s41598-025-30768-x.
35. Rusiecka, O.; Hrynkiewicz, K.; Trykowski, G.; Szewczyk, R.; Bernat, P. Enzymatic Biodegradation of Poly(Butylene Adipate-Co-Terephthalate) (PBAT) Microplastic by Trichoderma Harzianum KKP534. *Int. Biodeterior. Biodegrad.* **2026**, *213*, 106370. https://doi.org/10.1016/j.ibiod.2026.106370.
36. Obeid, A.T.; Nascimento, T.R. de L.; Agassi, A.C.; Almeida, A.Z.F.; Guedes, A.P. de M.A.; Alves, J.M.; Bombonatti, J.F.S.; Velo, M.M. de A.C. Niobium Oxyhydroxide as a Bioactive Agent and Reinforcement to a High-Viscosity Bulk-Fill Resin Composite. *J. Appl. Oral Sci.* **2024**, *32*, 1–11. https://doi.org/10.1590/1678-7757-2023-0278.
37. Awais, M.; Khursheed, S.; Tehreem, R.; Sirajuddin; Mok, Y.S.; Siddiqui, G.U. PH Regulated Rapid Photocatalytic Degradation of Methylene Blue Dye via Niobium-Nitrogen Co-Doped Titanium Dioxide Nanostructures under Sunlight. *Appl. Catal. A Gen.* **2022**, *643*, 118764. https://doi.org/10.1016/j.apcata.2022.118764.
38. Heitmann, A.P.; Patrício, P.S.O.; Coura, I.R.; Pedroso, E.F.; Souza, P.P.; Mansur, H.S.; Mansur, A.; Oliveira, L.C.A. Nanostructured Niobium Oxyhydroxide Dispersed Poly (3-Hydroxybutyrate) (PHB) Films: Highly Efficient Photocatalysts for Degradation Methylene Blue Dye. *Appl. Catal. B Environ.* **2016**, *189*, 141–150. https://doi.org/10.1016/j.apcatb.2016.02.031.
39. Khan, S.; Saifullah, A.; Zhang, Z.; Dhakal, H.N. Structure–Processing–Property Relationships in PVOH/PBAT Blends Plasticized with Dipentaerythritol, ε-Caprolactone, and Water. *ACS Omega* **2026**, *11*, 65331–65350. https://doi.org/10.1021/acsomega.6c07788.
40. da Silva, G.T.S.T.; Nogueira, A.E.; Oliveira, J.A.; Torres, J.A.; Lopes, O.F.; Ribeiro, C. Acidic Surface Niobium Pentoxide Is Catalytic Active for CO2 Photoreduction. *Appl. Catal. B Environ.* **2019**, *242*, 349–357. https://doi.org/10.1016/j.apcatb.2018.10.017.
41. Xiong, J.; Chen, B.; Gu, Z.; Liu, S.; Zong, M.H.; Wu, X.; Lou, W.Y. Hierarchically Open-Capsule Metal–Organic Frameworks via Controlled Etching for Enzyme Encapsulation. *Chem. Eng. J.* **2023**, *468*, 143622. https://doi.org/10.1016/j.cej.2023.143622.
42. Sebatine, P.J.; Shivani, R.B.; Sherin Celshia, S.; Muthamizh, S.; Arul varman, K.; Shanmugaraj, K.; Mohan Kumar, R. Fabrication of NiO/$V_2O_5$ nanocomposite as Photocatalyst for Cationic Dye Degradation and Its Pathway. *Ceram. Int.* **2025**, *51*, 50516–50529. https://doi.org/10.1016/j.ceramint.2025.08.282.
43. Abdullah, U.; Ali, M.; Pervaiz, E. An Inclusive Review on Recent Advancements of Cadmium Sulfide Nanostructures and Its Hybrids for Photocatalytic and Electrocatalytic Applications. *Mol. Catal.* **2021**, *508*, 111575. https://doi.org/10.1016/j.mcat.2021.111575.

44. Rizzo, L.; Koch, J.; Belgiorno, V.; Anderson, M.A. Removal of Methylene Blue in a Photocatalytic Reactor Using Polymethylmethacrylate Supported $TiO_2$ Nanofilm. *Desalination* **2007**, *211*, 1–9. https://doi.org/10.1016/j.desal.2006.02.081.
45. Benhabiles, O.; Mahmoudi, H.; Lounici, H.; Goosen, M.F.A. Effectiveness of a Photocatalytic Organic Membrane for Solar Degradation of Methylene Blue Pollutant. *Desalin. Water Treat.* **2016**, *57*, 14067–14076. https://doi.org/10.1080/19443994.2015.1061954.
46. Peters, R.F.D.M.; Dos Santos, P.A.M.; Machado, T.C.; Lopez, D.A.R.; Machado, Ê.L.; De Assis Lawisch Rodriguez, A. Photocatalytic Degradation of Methylene Blue Using $TiO_2$ Supported in Ceramic Material. *Eclet. Quim.* **2018**, *43*, 26–32. https://doi.org/10.26850/1678-4618eqj.v43.1.2018.p26-32.
47. de Carvalho, G.S.G.; de Siqueira, M.M.; do Nascimento, M.P.; de Oliveira, M.A.L.; Amarante, G.W. Nb2O5 Supported in Mixed Oxides Catalyzed Mineralization Process of Methylene Blue. *Heliyon* **2020**, *6*, e04128. https://doi.org/10.1016/j.heliyon.2020.e04128.

**Disclaimer/Publisher's Note:** The statements, opinions and data contained in all publications are solely those of the individual author(s) and contributor(s) and not of MDPI and/or the editor(s). MDPI and/or the editor(s) disclaim responsibility for any injury to people or property resulting from any ideas, methods, instructions or products referred to in the content.